

---

# Extremely Simple Activation Shaping for Out-of-Distribution Detection

---

Andrija Djurisić<sup>1</sup>

Nebojsa Bozanic<sup>1,2</sup>

Arjun Ashok<sup>1</sup>

Rosanne Liu<sup>1,3</sup>

## Abstract

The separation between training and deployment of machine learning models implies that not all scenarios encountered in deployment can be anticipated during training, and therefore relying solely on advancements in training has its limits. Out-of-distribution (OOD) detection is an important area that stress-tests a model's ability to handle unseen situations: *Do models know when they don't know?* Existing OOD detection methods either incur extra training steps, additional data or make nontrivial modifications to the trained network. In contrast, in this work, we propose an extremely simple, post-hoc, on-the-fly activation shaping method, **ASH**, where a large portion (e.g. 90%) of a sample's activation at a late layer is removed, and the rest (e.g. 10%) simplified or lightly adjusted. The shaping is applied at inference time, and does not require any statistics calculated from training data. Experiments show that such a simple treatment enhances in-distribution and out-of-distribution sample distinction so as to allow state-of-the-art OOD detection on ImageNet, and does not noticeably deteriorate the in-distribution accuracy. We release alongside the paper two calls for explanation and validation, encouraging collective participation to further validate and understand the discovery. Calls, video and code can be found at: <https://andrijazz.github.io/ash>.

## 1 Introduction

Machine learning works by iteration. We develop better and better training techniques (validated in a closed-loop validation setting) and once a model is trained, we observe problems, shortcomings, pitfalls and misalignment in deployment, which drive us to go back to modify or refine the training process. However, as we enter an era of large models, recent progress is driven heavily by the advancement of scaling, seen on all fronts including the size of models, data, physical hardware as well as team of researchers and engineers [20, 4, 37, 38, 49, 50]. As a result, it is getting more difficult to conduct multiple iterations of the usual train-deployment loop; for that reason *post hoc* methods that improve model capability *without* the need to modify training are greatly preferred. Methods like zero-shot learning [36], plug-and-play controlling [9], as well as feature post processing [14] combine general and flexible pretrained models with post hoc operations to create more adaptive models in various applications.

The out-of-distribution (OOD) generalization failure is one of such pitfalls often observed in deployment. The central question around OOD detection is "*Do models know when they don't know?*" Ideally, neural networks (NNs) after sufficient training should produce low confidence or high uncertainty measures for data outside of the training distribution. However, that's not always the case [44, 33, 16, 35, 3]. Differentiating OOD from in-distribution (ID) samples proves to be a much harder task than expected. Many attribute the failure of OOD detection to NNs being poorly calibrated, which has led to an impressive line of work improving calibration measures [14, 23, 32]. With all these efforts OOD detection has progressed vastly, however there's still room to establish a Pareto frontier that offers the best OOD detection and ID accuracy tradeoff: ideally, an OOD detection pipeline

---

<sup>1</sup>ML Collective. <sup>2</sup>Faculty of Technical Sciences, University of Novi Sad. <sup>3</sup>Google Research, Brain Team. Correspondence to [rosanneliu@google.com](mailto:rosanneliu@google.com).

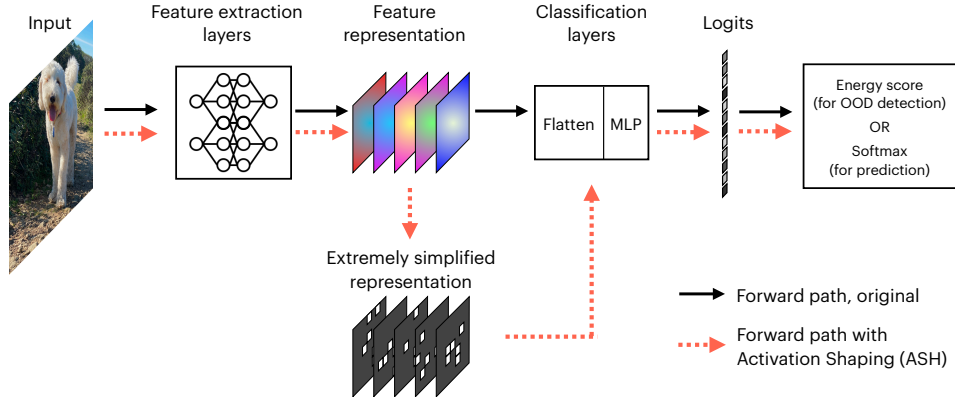


Figure 1: **Overview of the Activation Shaping (ASH) method.** ASH is applied to the forward path of an input sample. Black arrows indicate the regular forward path. Red dashed arrows indicate our proposed ASH path, adding one additional step to remove a large portion of the feature representation and simplify or lightly adjust the remaining, before routing back to the rest of the network. Note: we default to using the energy score calculated from logits for OOD detection, but the softmax score can also be used for OOD, and we have tested that in our ablation study.

should not deteriorate ID task performance, nor should it require a cumbersome parallel setup that handles the ID task and OOD detection separately.

A recent work, ReAct [42], observed that the unit activation patterns of a particular (penultimate) layer show significant difference between ID and OOD data, and hence proposed to rectify the activations at an upper limit—in other words, clipping the layer output at a certain value drastically improves the separation of ID and OOD data. A separate work, DICE [43], employs weight sparsification on a certain layer, and when combined with ReAct, achieves state-of-the-art on OOD detection on a number of benchmarks. Similarly, in this paper, we tackle OOD detection by making slight modifications to a pretrained network, assuming no knowledge of training or test data distributions. We show that an unexpectedly effective, and new state-of-the-art OOD detection can be achieved by a post hoc, one-shot *simplification* operation applied to input representations.

The extremely simple Activation **SH**aping (**ASH**) method takes an input’s feature representation (usually from a late layer) and perform a two-stage operation: 1) remove a large portion (e.g. 90%) of the activations based on a simple top-K criterion, and 2) adjust the remaining (e.g. 10%) activation values by scaling them up, or simply assigning them a constant value. The resulting, simplified representation is then populated throughout the rest of the network, generating scores for classification and OOD detection as usual. Figure 1 illustrates this process.

The hypothesis is that overparameterized neural networks produce excessive representations for inputs, which are likely largely redundant for the task at hand. In particular, to distinguish between ID and OOD samples, the full representations learned from a trained network are not as effective as their *simplified, cleaned* counterparts.

ASH is similar to ReAct [42] in its post-training, one-shot manner taken in the activation space in the middle of a network, and in its usage of the energy score for OOD detection. And similar to DICE [43], ASH performs a sparsification operation. However, we offer a number of advantages compared to ReAct: no global thresholds calculated from training data, and therefore completely *post hoc*; more flexible in terms of layer placement; better OOD detection performances across the board; better accuracy preservation on ID data, and hence establishing a much better Pareto frontier. As to DICE, we make no modification of the trained network whatsoever, and only operate in the activation space. Additionally, our method is plug-and-play, and can be combined with other existing methods, including ReAct (results shown in Table 5).

In the rest of the paper we develop and evaluate ASH via the following contributions:

- We propose an extremely simple, post-hoc and one-shot activation reshaping method, ASH, as a unified framework for both the original task and OOD detection (Figure 1).

- When evaluated across a suite of vision tasks including 3 ID datasets and 10 OOD datasets (Table 1), ASH immediately improves OOD detection performances across the board, establishing a new state of the art (SOTA), meanwhile providing the optimal ID-OOD trade-off, supplying a new Pareto frontier (Figure 2).
- We present extensive ablation studies on different design choices, including placements, pruning strength, and shaping treatments of ASH, while demonstrating how ASH can be readily combined with other methods, revealing the unexpected effectiveness and flexibility of such a simple operation (Section 5).
- We release two public calls for advancing both explanations and validations of our method, as a social experiment to establish a protocol for scientific communications and kick-starting collaborations (Section 7).

## 2 The Out-of-distribution Detection Setup

OOD detection methods are normally developed with the following recipe:

1. Train a model (e.g. a *classifier*) with some data—namely the **in-distribution (ID)** data.
2. After training, freeze the model parameters.
3. At inference time, feed the model **out-of-distribution (OOD)** data.
4. Turn the model into a *detector* by coming up with a **score** from the model’s output, to differentiate whether an input is ID or OOD.
5. Use various **evaluation metrics** to determine how well the detector is doing.

The highlighted keywords are choices to be made in every experimental setting for OOD detection. Our design choices for every step in this paper are explained below.

**Datasets and models (Steps 1-3)** We adopt an experimental setting representative of the previous SOTA: DICE (on CIFAR) and ReAct (on ImageNet). Table 1 summarizes datasets and model architectures used. For CIFAR-10 and CIFAR-100 experiments, we used the 6 OOD datasets adopted in DICE [43]: SVHN [34], LSUN-Crop [48], LSUN-Resize [48], iSUN [47], Places365 [51] and Textures [6], while the ID dataset is the respective CIFAR. The model used is a pretrained DenseNet-101 [18]. For ImageNet experiments, we inherit the exact setup from ReAct [42], where the ID dataset is ImageNet-1k, and OOD datasets include iNaturalist [45], SUN [46], Places365 [51], and Textures [6]. We used ResNet50 [15] and MobileNetV2 [39] network architectures. All networks are pretrained with ID data and never modified post-training; their parameters remain unchanged during the OOD detection phase.

ID Dataset	OOD Datasets	Model architectures
CIFAR10 [21]	SVHN [34], LSUN C [48], LSUN R [48], iSUN [47], Places365 [51] and Textures [6]	DenseNet-101 [18]
CIFAR100 [21]	SVHN [34], LSUN C [48], LSUN R [48], iSUN [47], Places365 [51] and Textures [6]	DenseNet-101 [18]
ImageNet [19]	iNaturalist [45], SUN [46], Places365 [51], Textures [6]	ResNet50 [15], MobileNetV2 [39]

Table 1: **Datasets and models in our OOD experiments.** We cover both moderate scale (CIFAR) and large scale (ImageNet) OOD benchmark settings, involving evaluations on up to 10 OOD datasets and 3 network architectures. The setting is directly inherited from DICE [43] and ReAct [42] for the ease of comparison.

**Detection scores (Step 4)** Commonly used score functions for OOD detection is the maximum/predicted class probability from a Softmax distribution directly out of the model ([16]; referred to as the Softmax score from here on), and the Energy score [29]. Both can be directly obtained from the model’s output (either the Softmax output, or the logit output). As the Energy score has been shown to outperform Softmax [29, 42], we default to using the former. In our ablation studies we present versions of our method combined with the Softmax score, as well as other methods (see Table 5). For a given input  $\mathbf{x}$  and a trained network function  $f$ , the energy function  $E(\mathbf{x}; f)$  maps the logit outputs from the network,  $f(\mathbf{x})$ , to a scalar:

$$E(\mathbf{x}; f) = -\log \sum_{i=1}^C \exp(f_i(\mathbf{x})) \quad (1)$$

where  $C$  is the number of classes and  $f_i(\mathbf{x})$  is the logit output of class  $i$ . The score used for OOD detection is the *negative energy score* so that ID samples produce a higher score, consistent with the convention. We compare our method with other scoring methods, e.g. Mahalanobis distance [24], as well as other advanced methods that build upon them: ODIN [26] (built upon the Softmax score), ReAct [42] and DICE [43] (built upon the Energy score).

**Evaluation metrics (Step 5)** We evaluate our method using threshold-free metrics for OOD detection standardized in Hendrycks & Gimpel [16]: (i) AUROC: the Area Under the Receiver Operating Characteristic curve; (ii) AUPR: Area Under the Precision-Recall curve; and (iii) FPR95: false positive rate—the probability that a negative (e.g. OOD) example is misclassified as positive (e.g. ID)—when the true positive rate is as high as 95% [26]. In addition to OOD metrics, we also evaluate each method on their ID performance, which in this case is the classification accuracy on in-distribution data, e.g. Top-1 accuracy on the ImageNet validation set. We aim to provide a unified framework that handles the original task and OOD detection altogether in a single path, minimizing the computational overhead of a model at deployment.

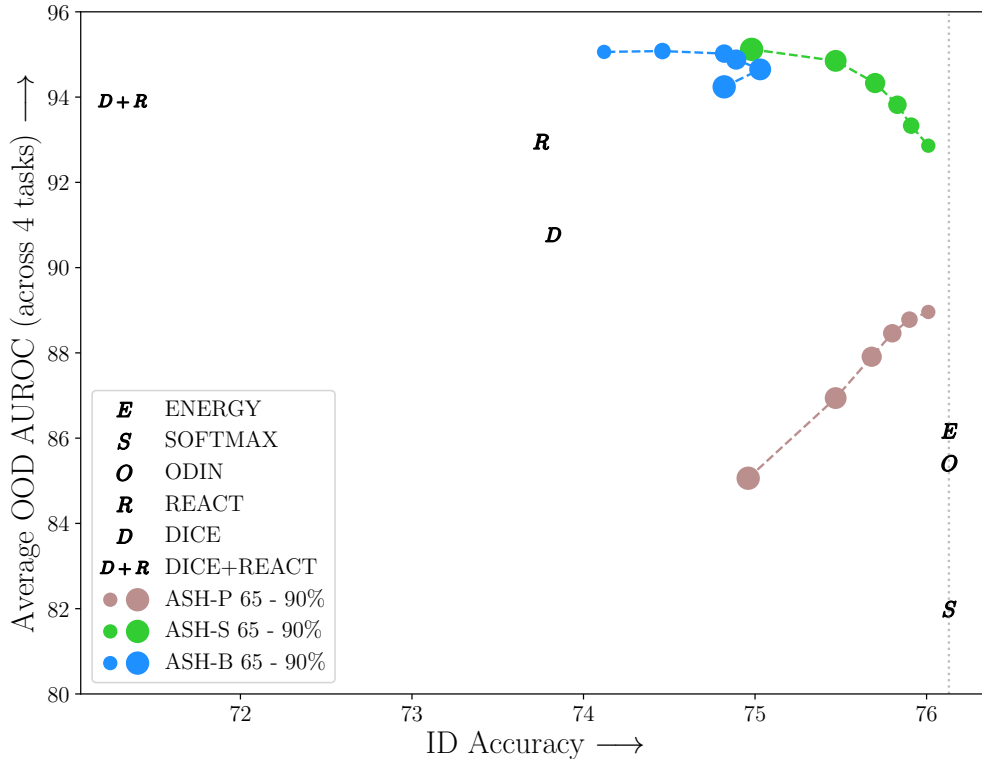


Figure 2: **ID-OOD tradeoff on ImageNet.** Plotted are the average OOD detection rate (AUROC; averaged across 4 OOD datasets) vs ID classification accuracy (Top-1 accuracy in percentage on ImageNet-1k validation set) of all OOD detection methods and their variants used in this paper. Baseline methods “E”, “S” and “O” lie on the upper bound of ID accuracy (indicated by the dotted gray line) since it makes no modification of the network or the features. “R”, “D” and “D+R” improve on the OOD metric, but come with an ID accuracy drop. ASH (dots connected with dashed lines; smaller dots indicate lower pruning level) offers the best trade-off and form a Pareto front.

### 3 Activation Shaping for OOD Detection

A trained network converts raw input data (e.g. RGB pixel values) into useful representations (e.g. a stack of spatial activations). We argue that representations produced by modern, over-parameterized deep neural networks are excessive for the task at hand, and therefore could be greatly simplified without much deterioration on the original performance (e.g. classification accuracy), while resulting in a surprising gain on other tasks (e.g. OOD detection).

Such a hypothesis is tested via an **activation shaping** method, ASH, which simplifies an input’s feature representation at a certain layer with the following recipe:

1. Remove a majority of the activation by obtaining the  $p$ th-percentile of the entire representation,  $t$ , and setting all values below  $t$  to 0.
2. For the un-pruned activations, apply one of the following treatments:
  - **ASH-P** (Algorithm 1): Do nothing. Pruning is all we need. This is used as a baseline to highlight the gains of the following two treatments.
  - **ASH-B** (Algorithm 2): Assign all of them to be a positive constant so the entire representation becomes **Binary**.
  - **ASH-S** (Algorithm 3): Scale their values up by a ratio calculated from the sum of activation values before and after pruning.

ASH is applied on-the-fly to any input sample’s feature representation at an intermediate layer, after which it continues down the forward path throughout the rest of the network, as depicted in Figure 1. Its output—generated from the simplified representation—is then used for both the original task (e.g. classification with the Softmax probabilities), or, in the case of OOD detection, obtaining a score, to which a thresholding mechanism is applied to distinguish between ID and OOD samples. ASH is therefore a unified framework for both the original task and OOD detection without incurring any additional path to the computational graph.

---

**Algorithm 1 ASH-P - Activation shaping with pruning**

---

**Input:** Single sample activation  $\mathbf{x}$ , pruning percentile  $p$

**Output:** Modified activation  $\mathbf{x}$

- 1: Calculate the  $p$ -th percentile of the input  $\mathbf{x} \rightarrow$  threshold  $t$
  - 2: Set every value in  $\mathbf{x}$  less than threshold  $t$  to zero
  - 3: **return**  $\mathbf{x}$
- 

---

**Algorithm 2 ASH-B - Activation shaping by binarizing**

---

**Input:** Single sample activation  $\mathbf{x}$ , pruning percentile  $p$

**Output:** Modified activation  $\mathbf{x}$

- 1: Calculate the sum of the input activation  $\mathbf{x} \rightarrow s$
  - 2: Calculate the  $p$ -th percentile of the input  $\mathbf{x} \rightarrow$  threshold  $t$
  - 3: Set every value in  $\mathbf{x}$  less than threshold  $t$  to zero
  - 4: Calculate the number of unpruned activation in  $\mathbf{x} \rightarrow n$
  - 5: Set every non-zero value in  $\mathbf{x}$  to  $s/n$
  - 6: **return**  $\mathbf{x}$
- 

**Placement of ASH** We can apply ASH at various places throughout the network, and the performance would differ. We found the most effective placements are towards the late layers of the network, for example, the penultimate layer (same as where ReAct [42] is applied). The main results shown in this paper are from applying ASH after the last average pooling layer in both ResNet50 and MobileNetV2, for ImageNet, where the feature map size is  $2048 \times 1 \times 1$  for ResNet50, and  $1280 \times 1 \times 1$  for MobileNetV2. For CIFAR experiments conducted with DenseNet-101, we apply ASH after the penultimate layer, where the feature size is  $342 \times 1 \times 1$ . Ablation studies for other ASH placements are included in Section 5 and Section A in Appendix.

---

**Algorithm 3** ASH-S - Activation shaping with scaling

---

**Input:** Single sample activation  $\mathbf{x}$ , pruning percentile  $p$

**Output:** Modified activation  $\mathbf{x}$

- 1: Calculate the sum of the input activation  $\mathbf{x} \rightarrow s1$
  - 2: Calculate the  $p$ -th percentile of the input  $\mathbf{x} \rightarrow$  threshold  $t$
  - 3: Set every value in  $\mathbf{x}$  less then threshold  $t$  to zero
  - 4: Calculate the sum of unpruned activation in  $\mathbf{x} \rightarrow s2$
  - 5: Multiply every non-zero value in  $\mathbf{x}$  with  $e^{\frac{s1}{s2}}$
  - 6: **return**  $\mathbf{x}$
- 

**The  $p$  parameter** ASH algorithms come with only one parameter,  $p$ : the percentage of activation values to prune. In experiments we generally vary  $p$  from 60 to 90 and have observed relatively steady performances (see Figure 2; the sam ASH variant with varying pruning levels are connected by a dashed line). When studying its effect on ID accuracy degradation, we cover the entire range from 0 to 100 (see Figure 3). The SOTA performances are given by surprisingly high values of  $p$ . For ImageNet, the best performing ASH versions are ASH-B with  $p = 65$ , and ASH-S with  $p = 90$ . For CIFAR-10 and CIFAR-100, the best performing ASH versions are ASH-S with  $p = 95$  and  $p = 90$ , and comparably, ASH-B with  $p = 95$  and  $p = 85$ . See Section D in Appendix for full details on the parameter choice.

## 4 Results

### 4.1 ASH offers the best ID-OOD tradeoff

ASH as a unified pipeline for both ID and OOD tasks demonstrates strong performance at both. Figure 2 shows the ID-OOD tradeoff of various methods for ImageNet. On one end, methods that rely on obtaining a score straight from the unmodified output of the network, e.g. Energy, Softmax and ODIN [26], perfectly preserves ID accuracy, but perform relatively poorly for OOD detection. Advanced methods that modify the network weights or representations, e.g. ReAct [42] and DICE [43], come at a compromise of ID accuracy when applied as one unified pipeline. In the case of ReAct [42], the ID accuracy drops from 76.13% to 73.75%.

ASH-B and ASH-S variants offer the best of both worlds: optimally preserve ID performance while improving OOD detection. Varying the pruning percentage  $p$ , we can see in Figure 2 that those ASH variants establish a new Pareto frontier. The pruning-only ASH-P gives the same ID accuracy as ASH-S at each pruning level, while falling behind ASH-S on the OOD metric, suggesting that simply by scaling up un-pruned activations, we obtain a great performance gain at OOD detection. The gain enlarges as we prune more and more of the activations.

### 4.2 OOD detection on both ImageNet and CIFAR benchmarks

ASH is highly effective at OOD detection. For ImageNet, while Figure 2 displays the averaged performance across 4 datasets tested, Table 2 lays out detailed performances on each of the datasets, and each of the two metrics: FPR95 and AUROC. The table follows the exact format with the same metrics reported in Sun *et al.* [42], reporting results from existing, competitive OOD detection methods in the literature, with additional baselines computed by us for a comprehensive comparison (e.g. DICE and DICE+ReAct on MobileNet). As we can see, the proposed ASH-B and ASH-S establish the new SOTA across almost all OOD datasets and evaluation metrics, while ASH-P showcases what improvements be achieve just by pruning (results shown in the table are obtained by simply removing 60% low value activations), outperforming Energy score, Softmax score and ODIN.

On CIFAR benchmarks, we followed the exact experimental setting as Sun & Li [43]: 6 OOD datasets with a pretrained DenseNet-101. Table 3 reports our methods' (averaged across all 6 datasets) performance alongside all baseline methods used in DICE [43]. Detailed per-dataset performance is reported in Table A2 and Table A3 in Appendix. All ASH variants profoundly outperform existing baselines.

		OOD Datasets									
Model	Methods	iNaturalist		SUN		Places		Textures		Average	
		FPR95 ↓	AUROC ↑	FPR95 ↓	AUROC ↑	FPR95 ↓	AUROC ↑	FPR95 ↓	AUROC ↑	FPR95 ↓	AUROC ↑
ResNet	Softmax score [16]	54.99	87.74	70.83	80.86	73.99	79.76	68.00	79.61	66.95	81.99
	ODIN [26]	47.66	89.66	60.15	84.59	67.89	81.78	50.23	85.62	56.48	85.41
	Mahalanobis [24]	97.00	52.65	98.50	42.41	98.40	41.79	55.80	85.01	87.43	55.47
	Energy score [29]	55.72	89.95	59.26	85.89	64.92	82.86	53.72	85.99	58.41	86.17
	ReAct [42]	20.38	96.22	24.20	94.20	33.85	91.58	47.30	89.80	31.43	92.95
	DICE [43]	25.63	94.49	35.15	90.83	46.49	87.48	31.72	90.30	34.75	90.77
	DICE + ReAct [43]	18.64	96.24	25.45	93.94	36.86	90.67	28.07	92.74	27.25	93.40
	ASH-P (Ours)	44.57	92.51	52.88	88.35	61.79	85.58	42.06	89.70	50.32	89.04
	<b>ASH-B (Ours)</b>	14.21	97.32	<b>22.08</b>	<b>95.10</b>	<b>33.45</b>	<b>92.31</b>	21.17	95.50	<b>22.73</b>	95.06
	<b>ASH-S (Ours)</b>	<b>11.49</b>	<b>97.87</b>	27.98	94.02	39.78	90.98	<b>11.93</b>	<b>97.60</b>	22.80	<b>95.12</b>
MobileNet	Softmax score [16]	64.29	85.32	77.02	77.10	79.23	76.27	73.51	77.30	73.51	79.00
	ODIN [26]	55.39	87.62	54.07	85.88	57.36	84.71	49.96	85.03	54.20	85.81
	Mahalanobis [24]	62.11	81.00	47.82	86.33	52.09	83.63	92.38	33.06	63.60	71.01
	Energy score [29]	59.50	88.91	62.65	84.50	69.37	81.19	58.05	85.03	62.39	84.91
	ReAct [42]	42.40	91.53	47.69	88.16	51.56	86.64	38.42	91.53	45.02	89.47
	DICE [43]	43.09	90.83	38.69	90.46	53.11	85.81	32.80	91.30	41.92	89.60
	DICE + ReAct [43]	32.30	93.57	<b>31.22</b>	<b>92.86</b>	<b>46.78</b>	<b>88.02</b>	16.28	96.25	<b>31.64</b>	<b>92.68</b>
	ASH-P (Ours)	54.92	90.46	58.61	86.72	66.59	83.47	48.48	88.72	57.15	87.34
	<b>ASH-B (Ours)</b>	<b>31.46</b>	<b>94.28</b>	38.45	91.61	51.80	87.56	20.92	95.07	35.66	92.13
	<b>ASH-S (Ours)</b>	39.10	91.94	43.62	90.02	58.84	84.73	<b>13.12</b>	<b>97.10</b>	38.67	90.95

Table 2: **OOD detection results on ImageNet.** We follow the exact same metrics and table format as Sun *et al.* [42]. Both ResNet and MobileNet are trained with ID data (ImageNet-1k) only.  $\uparrow$  indicates larger values are better and  $\downarrow$  indicates smaller values are better. All values are percentages. “DICE” and “DICE+ReAct” for MobileNet are implemented by us (refer to Section D for hyperparameter choices). The rest of the table except for those indicated “Ours” are taken directly from Table 1 in Sun *et al.* [42]. For ResNet, ASH consistently perform better than benchmarks, across all the OOD datasets. In the case of MobileNet, ASH performs comparably with DICE+ReAct.

Method	CIFAR-10		CIFAR-100	
	FPR95 ↓	AUROC ↑	FPR95 ↓	AUROC ↑
Softmax score [16]	48.73	92.46	80.13	74.36
ODIN [26]	24.57	93.71	58.14	84.49
Mahalanobis [24]	31.42	89.15	55.37	82.73
Energy score [29]	26.55	94.57	68.45	81.19
ReAct [42]	26.45	94.95	62.27	84.47
DICE [43]	20.83 $\pm$ 1.58	95.24 $\pm$ 0.24	49.72 $\pm$ 1.69	87.23 $\pm$ 0.73
<b>ASH-P (Ours)</b>	23.45	95.22	64.53	82.71
<b>ASH-B (Ours)</b>	20.23	96.02	48.73	88.04
<b>ASH-S (Ours)</b>	<b>15.05</b>	<b>96.61</b>	<b>41.40</b>	<b>90.02</b>

Table 3: **OOD detection results on CIFAR benchmarks.**  $\uparrow$  indicates larger values are better and  $\downarrow$  indicates smaller values are better. All values are percentages. Results are averaged across 6 OOD datasets. Methods except for ASH variants (marked as “Ours”) are taken from Sun & Li [43].

### 4.3 On preserving in-distribution accuracy

In this section, we discuss the intriguing fact that our method, when used as a unified pipeline for ID and OOD tasks, preserves in-distribution performance. We ask the central question:

*Why does making radical changes to a feature map, e.g. setting a large portion of activation values to 0, affect the accuracy so little?*

As we can see in Figure 2, towards the low end of pruning percentage (65%) both ASH-S and ASH-P come with only a slight drop of ID accuracy (ImageNet Top-1 validation accuracy; 76.13%

to 76.01%). The more we prune, the larger drop of ID accuracy is seen in ASH-S and ASH-P<sup>1</sup>. At 90%—that is, when 90% of activation values are eliminated—ASH-S and ASH-P maintain an in-distribution accuracy of 74.98%.

When experimenting with a wider range and granular pruning levels, as shown in Figure 3, we observe that ASH-S and ASH-P do preserve accuracy all the way, until a rather high value of pruning (e.g. ID accuracy dropped to 64.976% at 99% of pruning).

However, a reversed trend is observed in ASH-B: as seen in Figure 3, between 50-90% of pruning, the ID accuracy is trending up, while the best accuracy is achieved between 80% to 90% of pruned activation. The reason is that the rather extreme binarizing operation in ASH-B (setting all remaining activations to a constant) has a bigger impact when the pruning rate is lower (more values are being modified). To the extreme of 0% pruning, ASH-B simply sets all activation values to their average, which completely destroys the classifier (Figure 3, left end of curve).

We also notice that the effects of ASH-P and ASH-S on ID accuracy match exactly, validating that linearly scaling activations of the last layer and hence the logits, does not change the network output. Connecting back to Figure 2 and noticing the gap between ASH-P and ASH-S, we learned that such a simple scaling generates a large profit at OOD detection.

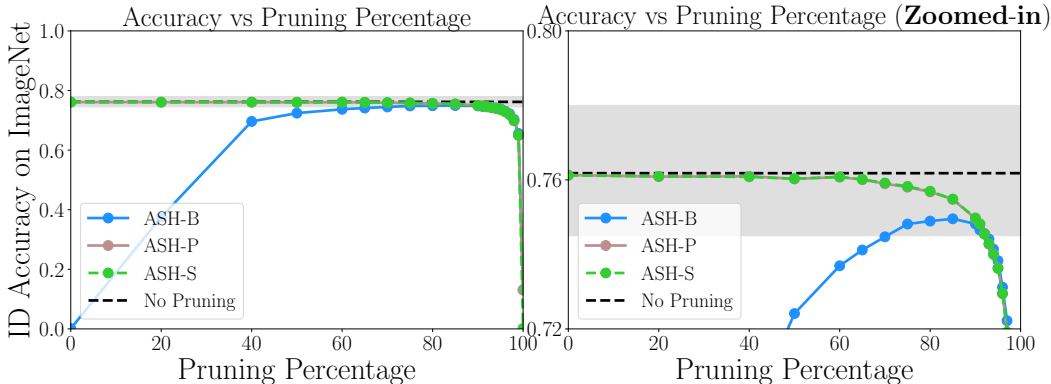


Figure 3: **Accuracy degradation on ImageNet across pruning percentage.** Here three versions of ASH are applied to the penultimate layer of a ResNet-50 pretrained on ImageNet. At test time the input samples from the ImageNet validation set are being processed with ASH, and the top-1 accuracy is reported across a range of pruning strength. ASH-P and ASH-S have the exact same effect on ID accuracy, as expected. ASH-B fails when pruning percentage is low, as the majority of the feature map will be converted to a constant value. The right plot is a zoomed-in version (on y axis) of the left.

#### 4.4 ASH-RAND: randomizing activation values

Given the success of ASH on both ID and OOD tasks, especially ASH-B where the values of a whole feature map are set to either 0 or a positive constant, we are curious to push the extent of activation shaping even further. We experiment with a rather extreme variant: ASH-RAND, which sets the remaining activation values to a random nonnegative value between  $[0, 10]$  after pruning. The result is shown in Table 4. It works reasonably well even for such an extreme modification of feature maps.

## 5 Discussion

In this section, we perform a number of ablation studies to understand the few design choices made in ASH, and we aim to provide various perspectives to understand the effectiveness of ASH.

**Global vs local threshold** The working version of ASH calculates the pruning threshold  $t$  (according to a fixed percentile  $p$ ; see Algorithms 1-3) per-image and on the fly, that is, each input

<sup>1</sup>ASH-P and ASH-S produce the exact accuracy on ID tasks, as linearly scaling the last-layer activation and hence logits, barring numerical instability, does not affect a model’s softmax output.



Method	ImageNet benchmark			
	FPR95	AUROC	AUPR	ID ACC
	↓	↑	↑	↑
ASH-RAND@65	45.37	90.80	98.09	72.16
ASH-RAND@70	46.93	90.67	98.05	72.87
ASH-RAND@75	46.93	90.67	98.05	73.19
ASH-RAND@80	51.24	89.94	97.89	73.57
ASH-RAND@90	59.35	87.88	97.44	73.51
Softmax score [16]	64.76	82.82	95.94	76.13
Energy score [29]	57.47	87.05	97.15	76.13
ODIN [26]	56.48	44.10	96.61	76.13
ASH-B@65	22.73	95.06	98.94	74.12
ASH-S@90	22.80	95.12	98.90	74.98

Table 4: **An extreme variant of ASH: randomizing activations.** ASH-RAND sets un-pruned activations to random values by drawing from a uniform distribution between 0 and 10. Pruning levels tested are between 65% and 90%. All experiments are based on the ImageNet benchmark with a pretrained ResNet-50, where the OOD performance shown are an average of 4 datasets. ↑ indicates larger values are better and ↓ indicates smaller values are better. All values are percentages. ASH-RAND is surprisingly comparable to, although not better than, ASH-B and ASH-S, whose best performing versions are included at the bottom. It consistently beats simple baselines like Energy, Softmax and ODIN.

image would have a pruning step applied with a different threshold. This design choice requires no global information of the network, training or test data, but incurs a slight overhead at inference. An alternative is to calculate a “global” threshold from all training data, assuming we still have access to them post training. There a 90% pruning level means gathering statistics of a certain feature map from all training data and obtaining a value that reflect the 90% percentile.

We implement both ASH-S and ASH-B with both global and local thresholds; the difference between the two design choices are showcased in Figure 4 for ASH-S. ASH-B results are included in Section C in Appendix. As we can see, with aligned pruning percentage, using a local threshold always works better than setting a global one, while the best overall performance is also achieved by local thresholds. Both threshold schemes produce a similar performance curve: performance metrics steadily increasing until starting to drop when too much features have been eliminated.

**Where to ASH** We notice that a working placement of ASH is towards later layers of a trained network, e.g. the penultimate layer. We experimented how other placements affect its performance. In Figure 5 we show the effect of performing ASH-S on different layers of a network—in this case a ResNet-50 on ImageNet. We can see that the accuracy deterioration over pruning rate becomes more severe as we move to earlier parts of the network. For full OOD detection results from these placements, refer to Section A in Appendix.

**Plug-and-play ASH to other methods** ASH as a two-step operation is very much compatible with other existing methods. In Table 5 we demonstrate how it can be easily combined with the Softmax score, the Energy score, ODIN and ReAct to provide immediate improvement over them. Experiments are performed with CIFAR-10, CIFAR-100 and ImageNet. All methods are reimplemented by us. See Section D in Appendix for implementation notes.

**How ASH changes the score distribution** One perspective to interpret the effectiveness of ASH is to examine how it morphs the score distribution to maximize separation between ID and OOD. Since we default to using Energy as the score function, we demonstrate how the energy score distributions change with different strength of ASH treatment, in Figure 6. From no ASH treatment (pruning: 0%) from the left plot to full treatment (90%) on the right, we can see how both ID and OOD distributions are morphed to maximize separation<sup>2</sup>.

<sup>2</sup>For animated plots, see: <https://andrijazz.github.io/ash/#dist>

Method	Local threshold			Global threshold		
	FPR95 ↓	AUROC ↑	AUPR ↑	FPR95 ↓	AUROC ↑	AUPR ↑
ASH-S@99	40.49	88.23	97.01	44.24	88.94	97.37
ASH-S@98	34.72	90.30	97.54	45.03	89.53	97.64
ASH-S@97	30.88	91.77	97.93	46.99	89.41	97.63
ASH-S@96	28.34	92.94	98.26	48.53	89.17	97.57
ASH-S@95	25.97	93.75	98.49	49.94	88.87	97.51
ASH-S@94	24.56	94.33	98.66	51.11	88.60	97.44
ASH-S@93	23.45	94.70	98.76	52.11	88.38	97.39
ASH-S@92	22.82	94.94	98.83	53.00	88.17	97.34
ASH-S@91	22.88	95.06	98.87	53.85	87.95	97.29
ASH-S@90	22.80	95.12	98.90	54.74	87.75	97.25
ASH-S@85	24.28	94.85	98.86	58.28	86.97	97.07
ASH-S@80	26.59	94.33	98.75	60.84	86.42	96.96
ASH-S@75	29.32	93.82	98.64	63.16	85.98	96.88
ASH-S@70	31.64	93.33	98.53	64.68	85.66	96.83

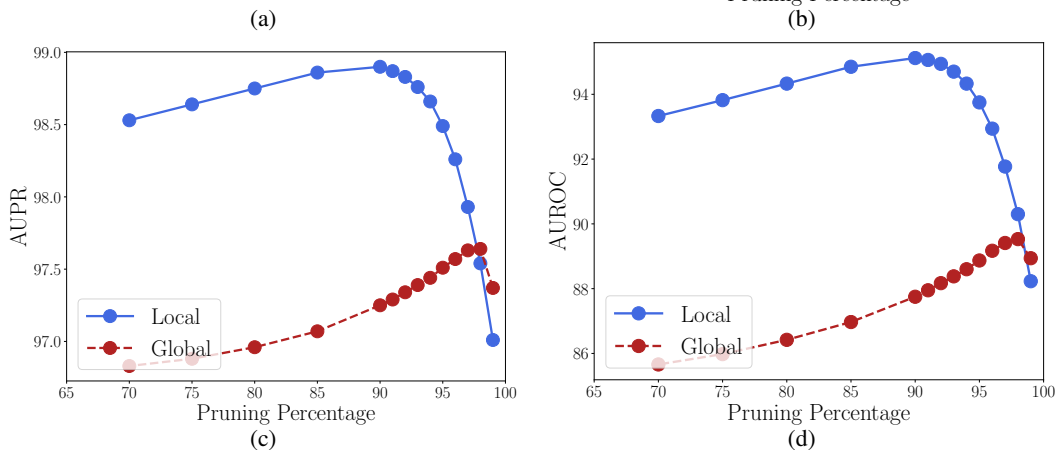


Figure 4: **Global vs local threshold.** We implement a variant of ASH with global thresholds obtained from training data, and compare the results with the defaulted local threshold version. Shown are ASH-S with a ResNet-50 trained on ImageNet. (a) Detailed results comparing local and global thresholds with a range of pruning percentage values and on three metrics. (b)-(d) Local vs global curves on FPR95, AUROC, and AUPR, respectively. Local thresholds, while incurring a slight overhead at inference, perform much better and require no access to training data.

Method	CIFAR-10			CIFAR-100			ImageNet		
	FPR95 ↓	AUROC ↑	AUPR ↑	FPR95 ↓	AUROC ↑	AUPR ↑	FPR95 ↓	AUROC ↑	AUPR ↑
Softmax score [16]	48.69	92.52	80.75	80.06	74.45	76.99	64.76	82.82	95.94
Softmax score + ASH	48.86	92.61	77.03	76.04	75.00	78.61	37.86	90.90	97.97
ODIN [26]	25.71	94.72	95.60	64.87	82.43	84.85	50.80	87.57	97.19
ODIN + ASH	15.38	96.41	96.62	38.54	90.49	91.51	28.59	93.34	98.40
Energy score [29]	26.59	94.63	95.61	68.29	81.23	83.64	57.47	87.05	97.15
Energy score + ASH	15.05	96.61	96.88	41.40	90.02	91.23	22.80	95.12	98.90
ReAct [42]	29.00	94.92	96.14	69.94	82.07	85.43	31.43	92.95	98.50
ReAct + ASH	16.35	96.91	97.41	41.64	88.93	90.14	24.88	94.27	98.66

Table 5: **ASH is compatible with and improves on existing methods.** ↑ indicates larger values are better and ↓ indicates smaller values are better. All values are percentages. CIFAR10 and CIFAR100 results are averaged across 6 different OOD tasks and ImageNet results are averaged across 4 different OOD tasks. All results are implemented by us.

**ASH as post hoc regularization** ASH can be thought of as a simple “feature cleaning” step, or a post hoc regularization of features. As we all now acknowledge that NNs are overparameterized, consequently, we can think of the representation learned by such networks as likely “overrepresented.” While the power of overparameterization shines mostly through making the training easier—adding more dimensions to the objective landscape while the intrinsic dimension of the task at hand remains

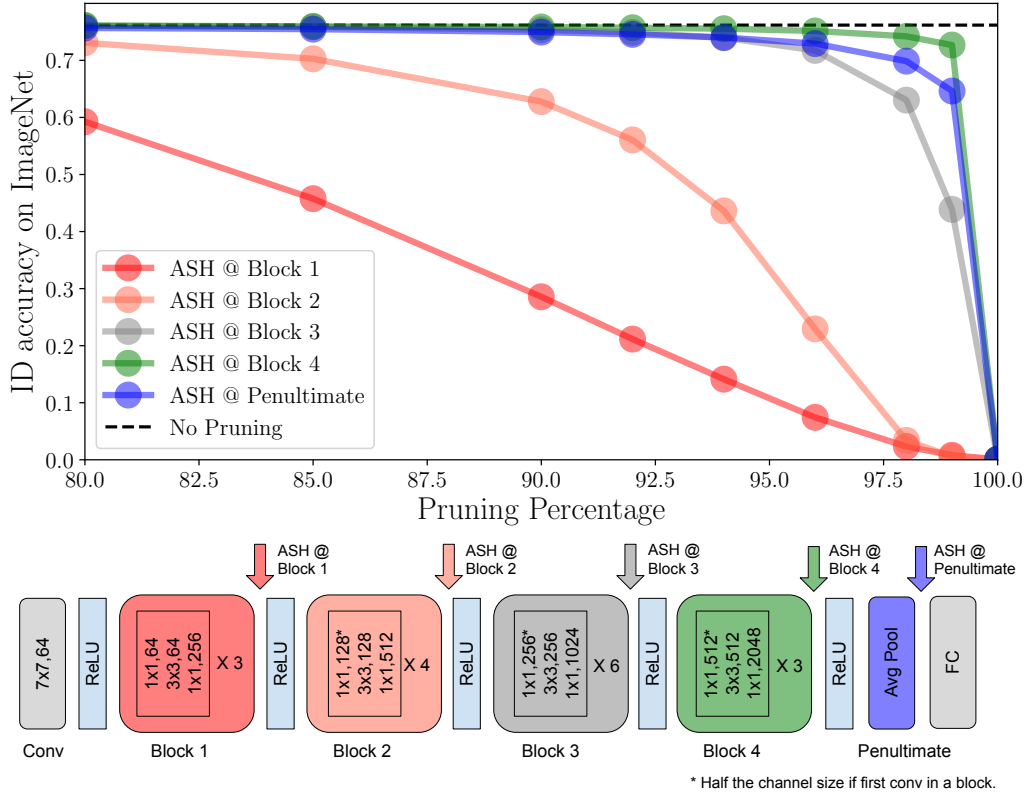


Figure 5: **Effect of ASH Placements on ID Accuracy.** (Top) ID accuracy degradation curves across pruning percentage, each color indicating a different placement of ASH. (Bottom) Diagram of a ResNet-50 architecture and indications of where ASH is applied. Experiments are done with ASH-S/P on ImageNet. Full results including the OOD performance can be seen in Section A in Appendix.

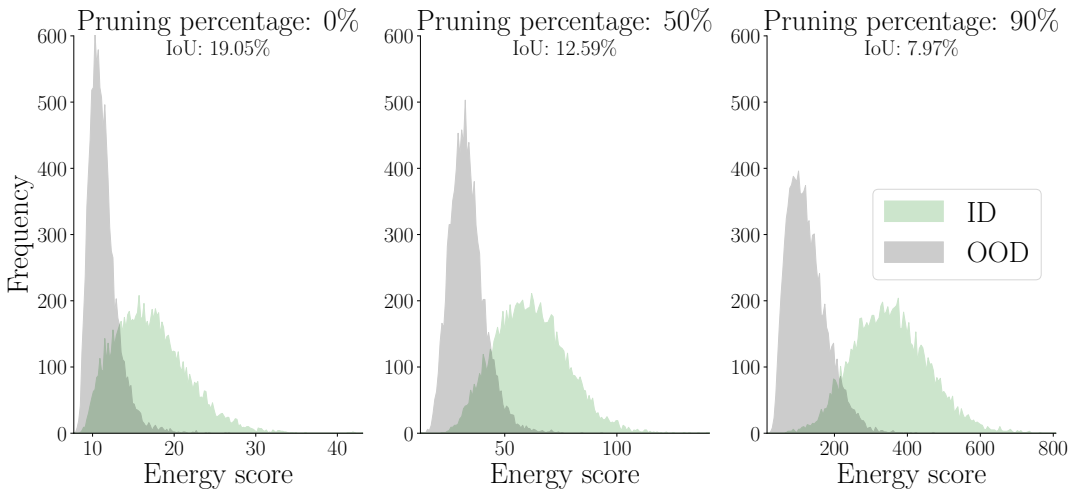


Figure 6: **Energy score distributions.** ASH with increasing pruning strength from left to right morphs the distributions of ID and OOD data, improving the separation, indicated by the Intersection Over Union (IoU) measure. ID data is ImageNet, and OOD data iNaturalist. Shown are energy scores without ASH (left), with ASH-S at 50% pruning strength (middle) and ASH-S at 90% (right).

constant [25], we argue that from the lens of representation learning, overparameterized networks “overdo” feature representation, i.e. the representation produced of an input contain too much

redundancy. We conjecture that a simple feature cleaning step post training can help ground the resulting learned representation better. Future work to validate, or invalidate this conjecture would include testing if simplified or regularized representation works well in other problem domains, from generalization, to transfer learning and continual learning.

**Connection to a modified ReLU** Another lens with which to interpret ASH is to see it as a modified ReLU function, adapted on-the-fly per input sample. Since we operate on feature activations pre-ReLU, as shown in Figure 7, the most basic version, ASH-P, combined with the subsequent ReLU function, becomes simply an adjusted ReLU. Since the cut-off is determined per-input and on-the-fly, it is essentially an data-dependent activation function. The success of ASH highlights the need to look into more flexible, adaptive, data-dependent activation functions at inference.

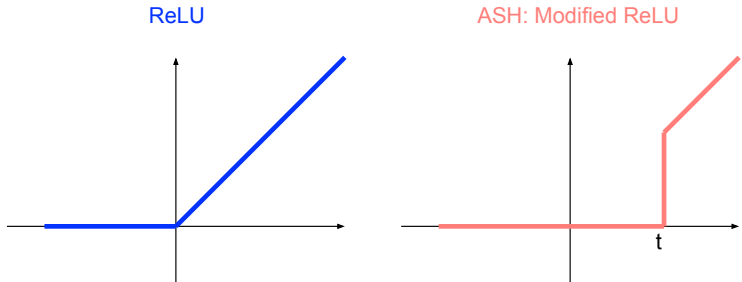


Figure 7: **ASH as a modified ReLU.** Comparison of a regular ReLU activation function (left) with a modified ReLU (right), which is equivalent to the ASH-P operation. The pruning threshold  $t$  is input data dependent, which makes ASH-P equivalent to a modified ReLU with adaptive thresholds.

**Magnitude vs value in pruning** Lots of existing pruning methods rely on the *magnitude* of a number (weights or activations). However in this work we use the direct values. That is, a large negative will be pruned if it is within the  $p$ -percentile of value distribution. The reason is that we operate on activations either *before ReLU*, in which case all negative values will be removed subsequently, or on the penultimate layer where all values are already non-negative.

## 6 Related Work

**Post-hoc model enhancement** Our method can be thought of as making post-hoc modifications to a trained network and how it handles input data for gains in OOD detection. Across various application domains similar practices have been incorporated for different purposes. For example, test-time augmentation of images via multiple crops and the averaging their predictions has been a common procedure since AlexNet [22] and VGG [41]. In the same vein, Monte Carlo dropout [12] estimates predictive uncertainty by adding dropout layers at test time, generating multiple predictions of for the same input instance. In adversarial defense, randomized smoothing and methods alike [7] applies random Gaussian perturbations of an input to obtain robust outputs. The downside of these methods is that they all require multiple inference runs per input image, and the gained advantage—whether on accuracy, calibration, or robustness—comes from the injected diversity from these runs.

The field of model editing [40, 30] also incorporate the idea of post-hoc model enhancement. In the field of fairness, trained models are often debiased via post-processing, where group-specific thresholding rules are adjusted to maximize accuracy subject to prescribed fairness guarantees [2, 5, 31, 8]. However, they all involve intense domain expertise as well as additional data, neither of which required in our work.

Temperature scaling [14] rescales the neural networks’ logits by a scalar learned from a separate validation dataset. In our case, we do not require access to any additional dataset, and the post processing is performed with a parameter set upfront, instead of learned. Applied to the OOD detection domain, and close to our work is ODIN [26], which combines temperature scaling and input

perturbations to achieve better detection. We have compared closely with ODIN in our experiments and have shown superior results.

In Dombrowski *et al.* [11] an explanation method is developed by replacing ReLU with Softplus in a trained model, achieving better model interpretability. All of these work repurpose trained models for other utilities, without accounting for their original task performance. ASH as a unified framework does not compromise performances on the original, trained tasks.

**Sparse representations** A parallel can be drawn between ASH and activation pruning, and the more general concept of sparse representations. Stochastic activation pruning (SAP) [10] has been proposed as a useful technique against adversarial attacks. SAP prunes a random subset of low-magnitude activations during each forward pass and scales up the others. This stochasticity reduces the impact an adversary has, and thereby allows the model to be robust under adversarial attacks. Adversarial defense is out of scope for this paper, but serves as a straightforward and fruitful future work direction. Ahmad & Scheinkman [1] used combinatorics of random vectors to show how sparse activations might enable units to use lower thresholds without risk of false positives, which can have a number of benefits like increased noise tolerance. They use top-K (without rescaling) in their network as an activation function, in place of ReLU. The key difference from ASH is that they use top-K even during training, and their theoretical arguments are based on the model being trained with sparse activations.

**Targeted dropout** Our method can also be interpreted through the lens of a targeted dropout on activations, instead of weights. Targeted dropout [13] is a method introduced to compress overparameterized machine learning models by dropping a set of units and weights that were stochastically selected from the set of the least important parameters (i.e. with the lowest magnitude), thus predicting which unit or weight may get pruned later [17]. A neural network trained using targeted dropout is shown to be extremely robust to post-hoc pruning of units and weights that repeatedly occur in the dropped set. Our method can be thought of as a targeted dropout on activations, and at test time.

## 7 Call for Explanation and Validation

We are releasing two calls alongside this paper to encourage, increase, and broaden the reach of scientific interactions and collaborations. The two calls are an invitation for fellow researchers to address two questions that are not yet sufficiently answered by this work:

- What are plausible explanations of the effectiveness of ASH, a simple activation pruning and readjusting technique, on ID and OOD tasks?
- Are there other research domains, application areas, topics and tasks where ASH (or a similar procedure) is applicable, and what are the findings?

Answers to these calls will be carefully reviewed and selectively included in future versions of this paper, where individual contributors will be invited to collaborate<sup>3</sup>. For each call we provide possible directions to explore the answer, however, we encourage novel quests beyond what's suggested below.

**Call for explanation** A plausible explanation of the effectiveness of ASH is that the knowingly overparameterized neural networks likely overdo representation learning—generating features for data that are largely redundant for the optimization task at hand. It is both an advantage and a peril: on the one hand the representation is less likely to overfit to a single task and might retain more potential to generalize, but on the other hand it serves as a poorer discriminator between data seen and unseen.

**Call for validation in other domains** We think adjacent domains that use a deep neural network (or any similar intelligent systems) to learn representations of data when optimizing for a training task would be fertile ground for validating ASH. A straightforward domain is natural language processing, where pretrained language models are often adapted for downstream tasks. Are native representations learned with those large language models simplifiable? Would reshaping of activations (in the case of

---

<sup>3</sup>Please follow instructions when submitting to the calls: <https://andrijazz.github.io/ash/#calls>

transformer-based language models, activations can be keys, values or queries) enhance or damage the performance?

## 8 Conclusion

In this paper, we present ASH, an extremely simple, post hoc, on-the-fly, and plug-and-play activation shaping method applied to inputs at the inference time. ASH works by pruning a large portion of an input sample’s activation and lightly adjusting the remaining. When combined with energy scores, it’s shown to outperform all contemporary methods for OOD detection, on both moderate and large-scale image classification benchmarks. The extensive experimental setup on 3 ID datasets, 10 OOD datasets, and performances evaluated on 4 metrics, demonstrates the effectiveness of ASH across the board: reaching SOTA on OOD detection while providing the best trade-off between OOD detection and ID classification accuracy.

The unexpected effectiveness of ASH calls for further investigations for understanding. To that end, the authors release two calls for collaborations on both the explanation and validation front, believing that science is best done as a collective endeavor. Submissions received for the calls will be carefully reviewed and contributions included in future versions of this paper.

## Acknowledgements

This work was supported in part by a computational grant to ML Collective funded by Google Cloud, and was selected by the ICLR 2022 DEI initiative [27, 28] as a sponsored project. The authors would like to thank Marcus Lewis for proofreading and supplying connections to the sparsity literature, and Milan Mistic for fruitful discussions and brainstorming in the early phase of the project. We thank the ML Collective community and the ICLR CoSubmitting Summer community for the ongoing support and feedback of this research.

## References

- [1] Subutai Ahmad and Luiz Scheinkman. “How can we be so dense? The benefits of using highly sparse representations”. In: *arXiv preprint arXiv:1903.11257* (2019).
- [2] Ibrahim M Alabdulmohsin and Mario Lucic. “A near-optimal algorithm for debiasing trained machine learning models”. In: *Advances in Neural Information Processing Systems* 34 (2021), pp. 8072–8084.
- [3] Dario Amodei et al. “Concrete problems in AI safety”. In: *arXiv preprint arXiv:1606.06565* (2016).
- [4] Tom B. Brown et al. *Language Models are Few-Shot Learners*. 2020. DOI: 10.48550/ARXIV.2005.14165. URL: <https://arxiv.org/abs/2005.14165>.
- [5] L Elisa Celis et al. “Classification with fairness constraints: A meta-algorithm with provable guarantees”. In: *Proceedings of the conference on fairness, accountability, and transparency*. 2019, pp. 319–328.
- [6] Mircea Cimpoi et al. “Describing textures in the wild”. In: *Proceedings of the IEEE conference on computer vision and pattern recognition*. 2014, pp. 3606–3613.
- [7] Jeremy Cohen, Elan Rosenfeld, and Zico Kolter. “Certified adversarial robustness via randomized smoothing”. In: *International Conference on Machine Learning*. PMLR. 2019, pp. 1310–1320.
- [8] Sam Corbett-Davies et al. “Algorithmic decision making and the cost of fairness”. In: *Proceedings of the 23rd acm sigkdd international conference on knowledge discovery and data mining*. 2017, pp. 797–806.
- [9] Sumanth Dathathri et al. “Plug and Play Language Models: A Simple Approach to Controlled Text Generation”. In: *International Conference on Learning Representations*. 2020. URL: <https://openreview.net/forum?id=H1edEyBKDS>.
- [10] Guneet S Dhillon et al. “Stochastic activation pruning for robust adversarial defense”. In: *arXiv preprint arXiv:1803.01442* (2018).
- [11] Ann-Kathrin Dombrowski et al. “Explanations can be manipulated and geometry is to blame”. In: *Advances in Neural Information Processing Systems*. Ed. by H. Wallach et al. Vol. 32. Curran Associates, Inc., 2019. URL: <https://proceedings.neurips.cc/paper/2019/file/bb836c01cdc9120a9c984c525e4b1a4a-Paper.pdf>.
- [12] Yarin Gal and Zoubin Ghahramani. “Dropout as a bayesian approximation: Representing model uncertainty in deep learning”. In: *international conference on machine learning*. PMLR. 2016, pp. 1050–1059.
- [13] Aidan N Gomez et al. “Learning sparse networks using targeted dropout”. In: *arXiv preprint arXiv:1905.13678* (2019).
- [14] Chuan Guo et al. “On calibration of modern neural networks”. In: *International conference on machine learning*. PMLR. 2017, pp. 1321–1330.
- [15] Kaiming He et al. “Deep residual learning for image recognition”. In: *Proceedings of the IEEE conference on computer vision and pattern recognition*. 2016, pp. 770–778.
- [16] Dan Hendrycks and Kevin Gimpel. “A Baseline for Detecting Misclassified and Out-of-Distribution Examples in Neural Networks”. In: *Proceedings of International Conference on Learning Representations* (2017).
- [17] Torsten Hoefler et al. “Sparsity in Deep Learning: Pruning and growth for efficient inference and training in neural networks”. In: *Journal of Machine Learning Research* 22.241 (2021), pp. 1–124.
- [18] Gao Huang et al. “Densely connected convolutional networks”. In: *Proceedings of the IEEE conference on computer vision and pattern recognition*. 2017, pp. 4700–4708.
- [19] Rui Huang and Yixuan Li. “Mos: Towards scaling out-of-distribution detection for large semantic space”. In: *Proceedings of the IEEE/CVF Conference on Computer Vision and Pattern Recognition*. 2021, pp. 8710–8719.
- [20] Jared Kaplan et al. *Scaling Laws for Neural Language Models*. 2020. DOI: 10.48550/ARXIV.2001.08361. URL: <https://arxiv.org/abs/2001.08361>.
- [21] Alex Krizhevsky, Geoffrey Hinton, et al. “Learning multiple layers of features from tiny images”. In: (2009).

- [22] Alex Krizhevsky, Ilya Sutskever, and Geoffrey E Hinton. “Imagenet classification with deep convolutional neural networks”. In: *Communications of the ACM* 60.6 (2017), pp. 84–90.
- [23] Balaji Lakshminarayanan, Alexander Pritzel, and Charles Blundell. “Simple and Scalable Predictive Uncertainty Estimation using Deep Ensembles”. In: *Advances in Neural Information Processing Systems*. Ed. by I. Guyon et al. Vol. 30. Curran Associates, Inc., 2017. URL: <https://proceedings.neurips.cc/paper/2017/file/9ef2ed4b7fd2c810847ffa5fa85bce38-Paper.pdf>.
- [24] Kimin Lee et al. “A simple unified framework for detecting out-of-distribution samples and adversarial attacks”. In: *Advances in neural information processing systems* 31 (2018).
- [25] Chunyuan Li et al. “Measuring the Intrinsic Dimension of Objective Landscapes”. In: *6th International Conference on Learning Representations, ICLR 2018, Vancouver, BC, Canada, April 30 - May 3, 2018, Conference Track Proceedings*. OpenReview.net, 2018. URL: <https://openreview.net/forum?id=ryup8-WCW>.
- [26] Shiyu Liang, Yixuan Li, and Rayadurgam Srikant. “Enhancing the reliability of out-of-distribution image detection in neural networks”. In: *arXiv preprint arXiv:1706.02690* (2017).
- [27] Rosanne Liu and Krystal Maughan. *Broadening Our Call for Participation to ICLR 2022*. 2021. URL: <https://blog.iclr.cc/2021/08/10/broadening-our-call-for-participation-to-iclr-2022> (visited on 09/19/2022).
- [28] Rosanne Liu and Krystal Maughan. *Reflection on the DEI Initiative at ICLR 2022*. 2022. URL: <https://blog.iclr.cc/2022/05/12/reflection-on-the-dei-initiative-at-iclr-2022/> (visited on 09/19/2022).
- [29] Weitang Liu et al. “Energy-based Out-of-distribution Detection”. In: *Advances in Neural Information Processing Systems (NeurIPS)*. 2020.
- [30] Kevin Meng et al. *Locating and Editing Factual Associations in GPT*. 2022. DOI: 10.48550/ARXIV.2202.05262. URL: <https://arxiv.org/abs/2202.05262>.
- [31] Aditya Krishna Menon and Robert C Williamson. “The cost of fairness in binary classification”. In: *Conference on Fairness, Accountability and Transparency*. PMLR. 2018, pp. 107–118.
- [32] Matthias Minderer et al. “Revisiting the calibration of modern neural networks”. In: *Advances in Neural Information Processing Systems* 34 (2021).
- [33] Seyed-Mohsen Moosavi-Dezfooli et al. “Universal adversarial perturbations”. In: *Proceedings of the IEEE conference on computer vision and pattern recognition*. 2017, pp. 1765–1773.
- [34] Yuval Netzer et al. “Reading digits in natural images with unsupervised feature learning”. In: (2011).
- [35] Anh Nguyen, Jason Yosinski, and Jeff Clune. “Deep neural networks are easily fooled: High confidence predictions for unrecognizable images”. In: 2015, pp. 427–436.
- [36] Alec Radford et al. “Learning transferable visual models from natural language supervision”. In: *International Conference on Machine Learning*. PMLR. 2021, pp. 8748–8763.
- [37] Aditya Ramesh et al. *Hierarchical Text-Conditional Image Generation with CLIP Latents*. 2022. arXiv: 2204.06125 [cs.CV].
- [38] Chitwan Saharia et al. *Photorealistic Text-to-Image Diffusion Models with Deep Language Understanding*. 2022. DOI: 10.48550/ARXIV.2205.11487. URL: <https://arxiv.org/abs/2205.11487>.
- [39] Mark Sandler et al. “Mobilenetv2: Inverted residuals and linear bottlenecks”. In: *Proceedings of the IEEE conference on computer vision and pattern recognition*. 2018, pp. 4510–4520.
- [40] Shibani Santurkar et al. “Editing a classifier by rewriting its prediction rules”. In: *Advances in Neural Information Processing Systems*. Ed. by M. Ranzato et al. Vol. 34. Curran Associates, Inc., 2021, pp. 23359–23373. URL: <https://proceedings.neurips.cc/paper/2021/file/c46489a2d5a9a9ecfc53b17610926ddd-Paper.pdf>.
- [41] Karen Simonyan and Andrew Zisserman. “Very deep convolutional networks for large-scale image recognition”. In: *arXiv preprint arXiv:1409.1556* (2014).
- [42] Yiyou Sun, Chuan Guo, and Yixuan Li. “ReAct: Out-of-distribution Detection With Rectified Activations”. In: ed. by M Ranzato et al. Vol. 34. Curran Associates, Inc., 2021, pp. 144–157. URL: <https://proceedings.neurips.cc/paper/2021/file/01894d6f048493d2cacde3c579c315a3-Paper.pdf>.
- [43] Yiyou Sun and Yixuan Li. “DICE: Leveraging Sparsification for Out-of-Distribution Detection”. In: *European Conference on Computer Vision*. 2022.



- [44] Christian Szegedy et al. “Intriguing properties of neural networks”. In: *arXiv preprint arXiv:1312.6199* (2013).
- [45] Grant Van Horn et al. “The inaturalist species classification and detection dataset”. In: *Proceedings of the IEEE conference on computer vision and pattern recognition*. 2018, pp. 8769–8778.
- [46] Jianxiong Xiao et al. “Sun database: Large-scale scene recognition from abbey to zoo”. In: *2010 IEEE computer society conference on computer vision and pattern recognition*. IEEE. 2010, pp. 3485–3492.
- [47] Pingmei Xu et al. “Turkergaze: Crowdsourcing saliency with webcam based eye tracking”. In: *arXiv preprint arXiv:1504.06755* (2015).
- [48] Fisher Yu et al. “Lsun: Construction of a large-scale image dataset using deep learning with humans in the loop”. In: *arXiv preprint arXiv:1506.03365* (2015).
- [49] Jiahui Yu et al. *Scaling Autoregressive Models for Content-Rich Text-to-Image Generation*. 2022. arXiv: 2206.10789 [cs.CV].
- [50] Susan Zhang et al. *OPT: Open Pre-trained Transformer Language Models*. 2022. DOI: 10.48550/ARXIV.2205.01068. URL: <https://arxiv.org/abs/2205.01068>.
- [51] Bolei Zhou et al. “Places: A 10 million image database for scene recognition”. In: *IEEE transactions on pattern analysis and machine intelligence* 40.6 (2017), pp. 1452–1464.

# Appendix: Extremely Simple Activation Shaping for Out-of-Distribution Detection

## A Full results on ASH placements

The main results shown in the paper are generated by placing ASH at later layers of the network: the penultimate layer for ResNet-50 and MobileNet. Here we show results if we place ASH at different locations of the network: 1st, 2nd, 3rd and 4th Block of ResNet-50, at the end of the last convolution layer at each block before the activation function (ReLU). Figure 5 (bottom) illustrates such placements, along with accuracy degradation curves (top). Here we show the OOD detection results from these ASH placements in Table A1.

As we can see, indeed the penultimate layer placement gives the best result in terms of ID accuracy preservation and OOD detection. As we move ASH towards the beginning of the network, both accuracy and OOD detection rates degrade.

It is worth noting that results in Table A1 adopt a different version of ASH for each layer block. For the penultimate layer and 4th Layer, we use ASH-S@90 (the same setting as that in the main paper), while for 1-3 Layers we use ASH-P@90. The reason is that ASH-S drastically degrades the performance. By simply adding a scaling factor (changing from ASH-P to ASH-S) on Layer 3, the ID accuracy drops from 75% to 5%.

ID: ImageNet; OOD: iNaturalist, Places, Textures, Sun				
ASH placement	FPR95 ↓	AUROC ↑	AUPR ↑	ID ACC ↑
ASH-P@90 before last ReLU of 1st Block	93.55	59.46	89.89	28.57
ASH-P@90 before last ReLU of 2nd Block	70.45	81.45	95.93	62.78
ASH-P@90 before last ReLU of 3rd Block	63.38	85.83	96.91	75.36
ASH-S@90 before last ReLU of 3rd Block	98.51	41.39	83.59	5.21
ASH-S@70 before last ReLU of 3rd Block	97.72	49.50	87.27	19.32
ASH-S@90 before last ReLU of 4th Block	34.69	92.11	98.38	75.83
ASH-S@90 after penultimate Layer*	22.80	95.12	98.90	74.98
No ASH (Energy score alone)	58.41	86.17	96.88	76.13

Table A1: **ASH applied to different places throughout a ResNet-50, trained on ImageNet.** OOD results are averaged across 4 different datasets/tasks: iNaturalist, Places, Textures, Sun. ↑ indicates larger values are better and ↓ indicates smaller values are better. All values are percentages. Experimental setup is described in Section 2

## B Detailed CIFAR results

Table A2 and Table A3 supplement Table 2 in the main text, as they display the full results on each of the 6 OOD datasets for models trained on CIFAR-10 and CIFAR-100 respectively.

## C ASH-B on ImageNet: Global vs local threshold

To complement the Figure 4 we provide comparison of global and local threshold for ASH-B Table A4.

## D Notes on implementation

All experiments are done with NVIDIA GTX1080Ti GPUs. Code to reproduce results is submitted alongside this appendix and can be found here: <https://github.com/andri jazz/ash>.

Notes on ImageNet results (Table 2):

- For both ResNet and MobileNet results, “ASH-P (Ours)” is implemented with  $p = 60$ , “ASH-B (Ours)” is implemented with  $p = 65$ , and “ASH-S (Ours)” is implemented with  $p = 90$ .

Table A2: Detailed results on six common OOD benchmark datasets: Textures [6], SVHN [34], Places365 [51], LSUN-Crop [48], LSUN-Resize [48], and iSUN [47]. For each ID dataset, we use the same DenseNet pretrained on CIFAR-10.  $\uparrow$  indicates larger values are better and  $\downarrow$  indicates smaller values are better.

Method	SVHN		LSUN-c		LSUN-r		iSUN		Textures		Places365		Average	
	FPR95	AUROC	FPR95	AUROC	FPR95	AUROC	FPR95	AUROC	FPR95	AUROC	FPR95	AUROC	FPR95	AUROC
Softmax score	$\downarrow$ 47.24	$\uparrow$ 93.48	$\downarrow$ 33.57	$\uparrow$ 95.54	$\downarrow$ 42.10	$\uparrow$ 94.51	$\downarrow$ 42.31	$\uparrow$ 94.52	$\downarrow$ 64.15	$\uparrow$ 88.15	$\downarrow$ 63.02	$\uparrow$ 88.57	$\downarrow$ 48.73	$\uparrow$ 92.46
ODIN	25.29	94.57	4.70	98.86	3.09	99.02	3.98	98.90	57.50	82.38	52.85	88.55	24.57	93.71
GODIN	6.68	98.32	17.58	95.09	36.56	92.09	36.44	91.75	35.18	89.24	73.06	77.18	34.25	90.61
Mahalanobis	6.42	98.31	56.55	86.96	9.14	97.09	9.78	97.25	21.51	92.15	85.14	63.15	31.42	89.15
Energy score	40.61	93.99	3.81	99.15	9.28	98.12	10.07	98.07	56.12	86.43	39.40	91.64	26.55	94.57
ReAct	41.64	93.87	5.96	98.84	11.46	97.87	12.72	97.72	43.58	92.47	43.31	91.03	26.45	94.67
DICE	$25.99 \pm 5.10$	$95.90 \pm 1.08$	$0.26 \pm 0.11$	$99.92 \pm 0.02$	$3.91 \pm 0.56$	$99.20 \pm 0.15$	$4.36 \pm 0.71$	$99.14 \pm 0.15$	$41.90 \pm 4.41$	$88.18 \pm 1.80$	$48.59 \pm 1.53$	$89.13 \pm 0.31$	$20.83 \pm 1.58$	$95.24 \pm 0.24$
ASH-P (Ours)	30.14	95.29	2.82	99.34	7.97	98.33	8.46	98.29	50.85	88.29	40.46	91.76	23.45	95.22
ASH-B (Ours)	17.92	96.86	2.52	99.48	8.13	98.54	8.59	98.45	35.73	92.88	48.47	89.93	20.23	96.02
ASH-S (Ours)	6.51	98.65	0.90	99.73	4.96	98.92	5.17	98.90	24.34	95.09	48.45	88.34	15.05	96.61

Table A3: Detailed results on six common OOD benchmark datasets: Textures [6], SVHN [34], Places365 [51], LSUN-Crop [48], LSUN-Resize [48], and iSUN [47]. For each ID dataset, we use the same DenseNet pretrained on CIFAR-100.  $\uparrow$  indicates larger values are better and  $\downarrow$  indicates smaller values are better.

Method	SVHN		LSUN-c		LSUN-r		iSUN		Textures		Places365		Average	
	FPR95	AUROC	FPR95	AUROC	FPR95	AUROC	FPR95	AUROC	FPR95	AUROC	FPR95	AUROC	FPR95	AUROC
Softmax score	$\downarrow$ 81.70	$\uparrow$ 75.40	$\downarrow$ 60.49	$\uparrow$ 85.60	$\downarrow$ 85.24	$\uparrow$ 69.18	$\downarrow$ 85.99	$\uparrow$ 70.17	$\downarrow$ 84.79	$\uparrow$ 71.48	$\downarrow$ 82.55	$\uparrow$ 74.31	$\downarrow$ 80.13	$\uparrow$ 74.36
ODIN	41.35	92.65	10.54	97.93	65.22	84.22	67.05	83.84	82.34	71.48	82.32	76.84	58.14	84.49
GODIN	36.74	93.51	43.15	89.55	40.31	92.61	37.41	93.05	64.26	76.72	95.33	65.97	52.87	85.24
Mahalanobis	22.44	95.67	68.90	86.30	23.07	94.20	31.38	93.21	62.39	79.39	92.66	61.39	55.37	82.73
Energy score	87.46	81.85	14.72	97.43	70.65	80.14	74.54	78.95	84.15	71.03	79.20	77.72	68.45	81.19
ReAct	83.81	81.41	25.55	94.92	60.08	87.88	65.27	86.55	77.78	78.95	82.65	74.04	62.27	84.47
DICE	$\downarrow$ 54.65 $\pm$ 4.94	$\uparrow$ 88.84 $\pm$ 0.39	$\downarrow$ 0.93 $\pm$ 0.07	$\uparrow$ 99.74 $\pm$ 0.01	$\downarrow$ 49.40 $\pm$ 1.99	$\uparrow$ 91.04 $\pm$ 1.49	$\downarrow$ 48.72 $\pm$ 1.55	$\uparrow$ 90.08 $\pm$ 1.36	$\downarrow$ 65.04 $\pm$ 0.66	$\uparrow$ 76.42 $\pm$ 0.35	$\downarrow$ 79.58 $\pm$ 2.34	$\uparrow$ 77.26 $\pm$ 1.08	$\downarrow$ 49.72 $\pm$ 1.69	$\uparrow$ 87.23 $\pm$ 0.73
ASH-P (Ours)	81.86	83.86	11.60	97.89	67.56	81.67	70.90	80.81	78.24	74.09	77.03	77.94	64.53	82.71
ASH-B (Ours)	53.52	90.27	4.46	99.17	48.38	91.03	47.82	91.09	53.71	84.25	84.52	72.46	48.73	88.04
ASH-S (Ours)	25.02	95.76	5.52	98.94	51.33	90.12	46.67	91.30	34.02	92.35	85.86	71.62	41.40	90.02

Method	Local threshold			Global threshold		
	FPR95 ↓	AUROC ↑	AUPR ↑	FPR95 ↓	AUROC ↑	AUPR ↑
ASH-B@99	45.43	89.09	97.55	41.70	89.75	97.55
ASH-B@98	39.59	91.22	98.08	41.64	90.57	97.87
ASH-B@97	36.54	92.17	98.30	42.73	90.57	97.88
ASH-B@96	34.26	92.79	98.44	43.55	90.43	97.85
ASH-B@95	32.64	93.20	98.52	44.38	90.20	97.79
ASH-B@94	31.09	93.51	98.59	45.39	89.99	97.75
ASH-B@93	30.03	93.76	98.64	45.77	89.86	97.72
ASH-B@92	29.01	93.95	98.68	46.29	89.71	97.68
ASH-B@91	28.43	94.10	98.71	46.97	89.55	97.64
ASH-B@90	27.58	94.24	98.74	48.25	89.39	97.61
ASH-B@85	25.26	94.65	98.83	51.04	88.77	97.48
ASH-B@80	24.04	94.88	98.88	53.63	88.24	97.37
ASH-B@75	22.95	95.02	98.91	56.66	87.63	97.25
ASH-B@70	22.39	95.08	98.93	60.19	86.93	97.12

Table A4: **Global vs local threshold.** Shown are ASH-B results with a ResNet-50 trained on ImageNet. Local threshold perform consistently better then global threshold.

- For the reimplementaion of DICE with MobileNet, we used a DICE pruning threshold of 70%.
- For reimplementing DICE + ReAct on MobileNet, since DICE and ReAct each come with their own hyperparameter, we tried a grid search, where DICE pruning thresholds include {10%, 15%, 70%} and ReAct clipping thresholds {1.0, 1.5, 1.33}. Rationals for choosing those values for grid search are: 10% and 15% are taken from the hyperparameter setup in the DICE codebase<sup>4</sup>, and 70% is the recommended threshold of DICE when used alone. In the case of ReAct clipping thresholds, 1.0 and 1.5 are taken from the same codebase, while 1.33 is the 90% percentile calculated from training data, following the ReAct procedure. We report the best result out of all the hyperparameter combinations, given by 10% DICE pruning and 1.0 ReAct clipping.

Notes on CIFAR results (Table 3, Table A2, Table A3):

- For CIFAR-10, ‘ASH-P (Ours)’ is implemented with  $p = 90$ , ‘ASH-B (Ours)’ is implemented with  $p = 95$ , and ‘ASH-S (Ours)’ is implemented with  $p = 95$ .
- For CIFAR-100, ‘ASH-P (Ours)’ is implemented with  $p = 80$ , ‘ASH-B (Ours)’ is implemented with  $p = 85$ , and ‘ASH-S (Ours)’ is implemented with  $p = 90$ .
- Results for other methods are copied from DICE.

Notes on compatibility results (Table 5):

- ‘‘Softmax score + ASH’’ is implemented with ASH-P @  $p = 95$  for CIFAR-10, ASH-B @  $p = 70$  for CIFAR-100, and ASH-B @  $p = 65$  for ImageNet.
- ‘‘Energy score + ASH’’ is implemented with ASH-S @  $p = 95$  for CIFAR-10, ASH-S @  $p = 90$  for CIFAR-100, and ASH-S @  $p = 90$  for ImageNet.
- ‘‘ODIN’’ and ‘‘ODIN + ASH’’ use a pretrained DenseNet-101 for CIFAR, where the magnitude parameter is 0.0028, and a pretrained ResNet-50, where the magnitude parameter is 0.005.

<sup>4</sup><https://github.com/deeplearning-wisc/dice/blob/4d393c2871a80d8789cc97c31adcee879fe74b29/demo-imagenet.sh>

- “ODIN + ASH” is implemented with ASH-S @  $p = 95$  for CIFAR-10, ASH-S @  $p = 90$  for CIFAR-100, and ASH-S @  $p = 90$  for ImageNet.
- “ReAct” results for CIFAR-10 and CIFAR-100 are implemented by us. We are unable to replicate the exact results shown in the DICE paper supplementary Table 9.
- “ReAct + ASH” is implemented with ASH-S @  $p = 90$  and ReAct clipping threshold of 1.0 for all of CIFAR-10, CIFAR-100, and ImageNet.